LCC – 0047 08//00
LCLS-TN-00-12

Linear Collider Collaboration Tech Notes

A Transverse RF Deflecting Structure for Bunch Length and Phase Space Diagnostics

August 2000

Paul Emma, Josef Frisch, Patrick Krejcik

Stanford Linear Accelerator Center
Stanford, CA

Abstract: A traveling wave transverse rf deflecting structure is discussed as a tool for bunch length measurement and as an aid to detailed phase space diagnostics in future FEL and linear collider projects. The idea is an old one [1], [2], but the applications are new. The high frequency time variation of the deflecting fields is used to 'pitch' or 'yaw' the electron bunch where the resulting transverse beam width measured on a simple profile monitor represents a reliable, single-shot measure of the absolute bunch length. A small rf phase shift, from the zero-crossing, adds a net centroid kick so that the bunch may intercept an off-axis screen. The deflecting rf is then pulsed at a much lower rate than the machine rate, and a pulse-stealing process is used to monitor the bunch length continuously. Multiple screens at appropriate phase advance locations might also be used to monitor the 'slice' (i.e. time-correlated) transverse emittance [3]. A screen placed at a point of significant momentum dispersion can also be used to reveal how longitudinal phase space is populated. Suitable S-band structures were built and tested in the 1960's at SLAC [4] and are available today. Simulations of these schemes are presented for the Linac Coherent Light Source [5], the existing SLAC linac, and the Next Linear Collider [6].

A Transverse RF Deflecting Structure for Bunch Length and Phase Space Diagnostics

Paul Emma, Josef Frisch, Patrick Krejcik
SLAC
August 29, 2000

ABSTRACT

A traveling wave transverse rf deflecting structure is discussed as a tool for bunch length measurement and as an aid to detailed phase space diagnostics in future FEL and linear collider projects. The idea is an old one [1], [2], but the applications are new. The high frequency time variation of the deflecting fields is used to 'pitch' or 'yaw' the electron bunch where the resulting transverse beam width measured on a simple profile monitor represents a reliable, single-shot measure of the absolute bunch length. A small rf phase shift, from the zero-crossing, adds a net centroid kick so that the bunch may intercept an off-axis screen. The deflecting rf is then pulsed at a much lower rate than the machine rate, and a pulse-stealing process is used to monitor the bunch length continuously. Multiple screens at appropriate phase advance locations might also be used to monitor the 'slice' (i.e. time-correlated) transverse emittance [3]. A screen placed at a point of significant momentum dispersion can also be used to reveal how longitudinal phase space is populated. Suitable S-band structures were built and tested in the 1960's at SLAC [4] and are available today. Simulations of these schemes are presented for the Linac Coherent Light Source [5], the existing SLAC linac, and the Next Linear Collider [6].

1 Introduction

One of the many technical challenges for future free-electron lasers (FEL) and linear colliders is the measurement and diagnosis of their extremely short electron bunches. The rms bunch length in the Linac Coherent Light Source (LCLS) [5] is 80 fsec (24 μm) and that of the Next Linear Collider (NLC) [6] is 300 fsec (90 μm). This is well beyond the range of streak cameras, but a similar concept can be applied by directly 'streaking' the electron beam using an rf deflecting field. This idea has been used in the past [1], [2] and has been suggested again recently [7]. The high frequency time variation of the deflecting fields is used to 'pitch' or 'yaw' the electron bunch, where the resulting transverse beam width measured on a simple profile monitor represents a reliable, single-shot measure of the absolute bunch length. Since the method effectively converts one of the profile monitor's transverse dimensions into time, the bunch can be analyzed in detail, revealing important time-correlations in the other phase space dimensions and allowing the 'time-sliced' rms dimensions of the beam to be measured. This can be an essential diagnostic in future FEL's where the time-sliced beam widths are of fundamental importance, and the long-term stability of these parameters needs continuous monitoring.

Suitable S-band traveling wave structures were built and tested in the 1960's at SLAC [4] and are still available today. These are 8-foot and 12-foot long structures capable of 25-30 MW of peak input power and up to 32 MV of peak deflecting voltage. Such structures can be utilized for future machines and even as a basic diagnostic in the existing SLAC linac. The following describes the relative effectiveness of the structures for any particular electron beam.

2 The Deflecting Structure

The existing S-band deflecting structures are described in references [1] and [4]. The disk-loaded waveguide structure is fabricated from brazed stacks of machined copper cylinders with a period of 3.5 cm. The iris radius is 2.24 cm, which is almost twice that of the accelerating structures. A cut-away view of the deflecting structure is shown in Figure 1. The polarization plane of the TM_{11} mode is determined by the orientation of the input coupler. Since minor imperfections in the structure could cause the mode to rotate, two additional holes are provided on either side of each iris to stabilize the mode and prevent rotations.

The structure has a $2\pi/3$ phase shift per cell, as shown in Figure 2. The field distribution of the TM_{11} produces a maximum transverse deflecting field in one cell, the same, with a sign reversal, in the next adjacent cell, and finally only a longitudinal field in the third

cell (see Figure 2). Note that the longitudinal field component is proportional to displacement from the axis and changes sign, passing through zero as one crosses the axis [see Eq. (2)].

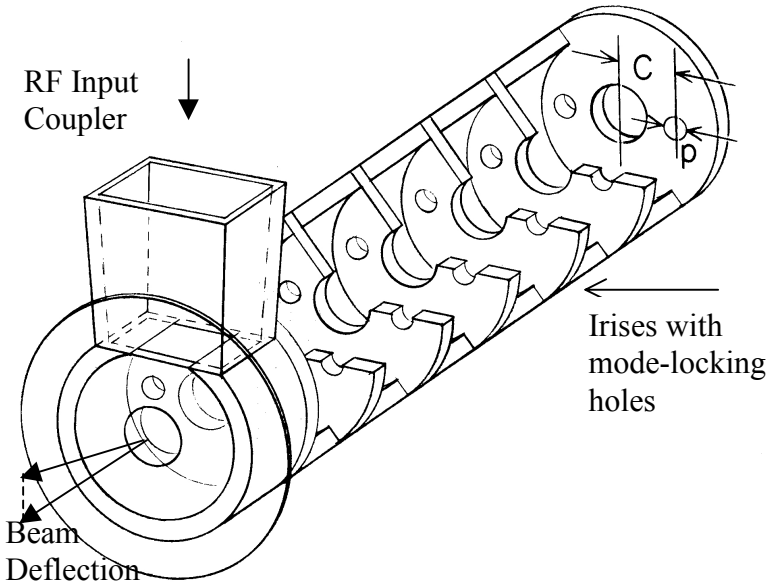

Figure 1. Schematic of a SLAC S-band transverse deflecting structure. The kick is vertical in this drawing.

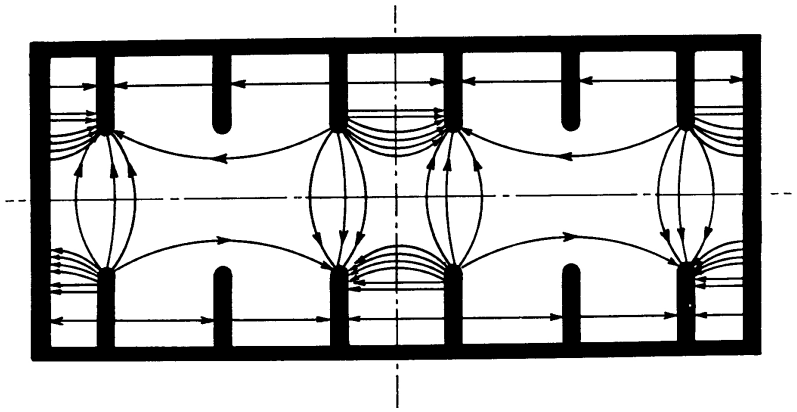

Figure 2. Time snap-shot of the field distribution of the TM_{11} mode with a $2\pi/3$ cell length.

At SLAC, there exists both 8-foot (2.44 m) and 12-foot (3.64 m) long structures, although we confine our consideration here to the 8-foot structures. Measurements [8] and calculations [9] of the deflection versus power indicate a power to voltage relationship of

$$V_0 \approx \left(1.6\ \text{MV/m/MW}^{1/2}\right) L\sqrt{P_0}\,, \tag{1}$$

where L is the structure length and P_0 is the peak input power.

Reference [4] describes the fields in the structures and makes an important point about the net forces, which we repeat here. The first-order solution for the lowest-order deflecting mode, in cylindrical coordinates, is given by

$$\begin{aligned} E_r &= E_0\left[\left(\tfrac{1}{2}kr\right)^2+\left(\tfrac{1}{2}ka\right)^2\right]\cos\theta \\ E_\theta &= E_0\left[\left(\tfrac{1}{2}kr\right)^2-\left(\tfrac{1}{2}ka\right)^2\right]\sin\theta \\ E_z &= iE_0kr\cos\theta \\ Z_0H_r &= -E_0\left[\left(\tfrac{1}{2}kr\right)^2-\left(\tfrac{1}{2}ka\right)^2+1\right]\sin\theta \\ Z_0H_\theta &= E_0\left[\left(\tfrac{1}{2}kr\right)^2+\left(\tfrac{1}{2}ka\right)^2-1\right]\cos\theta \\ Z_0H_z &= -iE_0kr\sin\theta \end{aligned} \tag{2}$$

where $k = 2\pi/\lambda$ is the free-space wave number, a is the radius of the iris, Z_0 is free-space impedance, $i=\sqrt{-1}$, $E_0 = |E_0|e^{ik(z-ct)}$ represents a traveling wave, and c is the speed of light. From the Lorentz force on a particle of charge e, one obtains the forces in rectangular coordinates.

$$\begin{aligned} F_x &= eE_0 \\ F_y &= 0 \\ F_z &= ieE_0kr\cos\theta \end{aligned} \tag{3}$$

The transverse deflecting field is uniform in magnitude and direction over the aperture, which implies an aberration-free deflection from this mode. The longitudinal force is 90° out of phase and depends linearly on radius, r. It is typically insignificant, even for values of r approaching a few millimeters.

The time averaged power transmitted through the structure is given by the real part of the integral over the aperture surface, S, of one-half of the normal component of the complex Poynting vector $\mathbf{E}\times\mathbf{H}^*$.

$$P = \frac{1}{2}\mathrm{Re}\left\{\oint_S \mathbf{E}\times\mathbf{H}^*\cdot d\mathbf{S}\right\} \tag{4}$$

Using the divergence theorem and the solution for the deflecting mode in equations (2) one obtains

$$P_z = \frac{\pi a^2}{2}\frac{|E_0|^2}{Z_0}\left(\frac{ka}{2}\right)^2\left[\frac{4}{3}\left(\frac{ka}{2}\right)^2 - 1\right]. \tag{5}$$

For the SLAC deflecting structure with $a = 2.24$ cm, the term in the square bracket is negative, indicating a backward wave mode. Consequently the rf power is fed in at the coupler at the downstream end of the structure.

3 Description of the Method

The aberration-free deflecting force imparts a transverse momentum on the bunch which varies in time over the passage of the bunch. The small kick angle, $\Delta x'$ ($<< 1$), as a function of longitudinal position along the bunch, z, is given approximately by

$$\Delta x'(z) = \frac{eV_0}{pc}\sin(kz + \varphi) \approx \frac{eV_0}{p_z c}\left[\frac{2\pi}{\lambda} z\cos\varphi + \sin\varphi\right], \tag{6}$$

where V_0 is the peak voltage, p is the beam's longitudinal momentum in the structure, and φ is the rf phase (= 0 at zero-crossing). The approximation is made that $|z| << \lambda/2\pi$, so only the linear term in z is retained. We have ignored the fact that the electric field actually increases the total beam momentum by accelerating in the transverse direction. The typical effect on the momentum is tiny and is estimated by $\Delta p/p \approx \Delta x'^2/2$.

From Eq. (6) it is clear that a centroid deflection occurs for $\sin\varphi \neq 0$ and an *angular* 'yaw' (or 'pitch' for a vertical deflector) is generated along the bunch which is linear in z. A *spatial* 'pitch' arises at a screen placed downstream of the deflector, where the beam has been transported through a transfer matrix with angular-to-spatial element $R_{12} = (\beta_d\beta_s)^{1/2}\sin\Delta\psi$. Here, β_d is the beta function at the deflector, β_s is the beta function at the screen, and $\Delta\psi$ is the betatron phase advance from deflector to screen. The transverse position of each ultra-relativistic electron on the screen is then given by

$$\Delta x(z) \approx \frac{eV_0}{pc}\sqrt{\beta_d\beta_s}\,\sin\Delta\psi\left(\frac{2\pi}{\lambda} z\cos\varphi + \sin\varphi\right). \tag{7}$$

Taking the mean value over the ensemble of particles, for the nominal case with $\langle z\rangle = 0$, gives the transverse centroid offset at the screen.

$$\langle\Delta x\rangle = \frac{eV_0}{pc}\sqrt{\beta_d\beta_s}\,\sin\Delta\psi\sin\varphi \tag{8}$$

Similarly, the rms beam size on the screen is

$$\left\langle \left(x - \langle x \rangle \right)^2 \right\rangle^{1/2} \equiv \sigma_x = \sqrt{\sigma_{x0}^2 + \sigma_z^2 \beta_d \beta_s \left(\frac{2\pi e V_0}{\lambda pc} \sin\Delta\psi \cos\varphi \right)^2} \,, \tag{9}$$

where σ_{x_0} is the nominal beam size on the screen (*i.e.* in the absence of a deflecting voltage), and σ_z (= $\langle z^2 \rangle^{1/2}$) is the rms bunch length.

If the rf voltage is adequate, the beam size associated with the bunch length will dominate the nominal beam size, and the quadrature addition in Eq. (9) becomes a small correction. This requires that the rf deflecting voltage be large compared to the scaled nominal beam size, or

$$|eV_0| \gtrsim \frac{\lambda}{\pi\sigma_z} \frac{1}{|\sin\Delta\psi \cos\varphi|} \sqrt{pc \cdot mc^2 \frac{\varepsilon_N}{\beta_d}} \,, \tag{10}$$

which, when Eq. (10) is in equality, results in a quadrature correction of just 12.5 %. Here we have used, for the screen's nominal spot size,

$$\sigma_{x_0} = \sqrt{\beta_s \varepsilon_N / \gamma} \,, \tag{11}$$

where γ (= pc/mc^2) is the Lorentz energy factor, mc^2 is the electron rest energy, and ε_N is the normalized transverse rms emittance (in the deflection plane). Eq. (10) indicates that the required voltage scales weakly with the square-root of beam momentum and inversely with bunch length. The required voltage also decreases with smaller emittance and decreases for larger values of the beta function in the deflector. The beta function at the screen does not effect the 'signal-to-noise' relationship of Eq. (10), but it does scale the measured spot size in Eq. (9). Similarly, a phase advance near $\pi/2$ and an rf phase near zero-crossing are advantageous. Finally, a shorter rf wavelength also reduces the voltage required. For S-band ($\lambda \approx 10.5$ cm) and example LCLS parameters ($pc \approx 5$ GeV, $\sigma_z \approx 24$ μm, $\varepsilon_N \approx 1$ μm, $\beta_d \approx 50$ m), the deflector voltage should be $|V_0| \geq 10$ MV.

The possibility of acceleration between the deflecting structure and the screen should also be incorporated into these relationships. This is included by everywhere replacing the beta function product with

$$\beta_d \beta_s \rightarrow \beta_d \beta_s \, E_d / E_s \,, \tag{12}$$

where E_d ($\approx pc$) is the beam energy in the deflector and E_s is the energy at the screen. Including acceleration, the measured bunch length is calculated using Eq. (9).

$$\sigma_z = \frac{\lambda}{2\pi} \frac{\sqrt{E_d E_s}}{|eV_0 \sin\Delta\psi \cos\varphi|} \sqrt{\frac{\left(\sigma_x^2 - \sigma_{x_0}^2 \right)}{\beta_d \beta_s}} \tag{13}$$

4 Wakefields and Second-Order Effects

An *x*-*z* (or *y*-*z*) correlation along the bunch is influenced by three main effects. The first of these is the transverse rf deflections described in Eq. (7). The second is the transverse wakefields of the accelerating structures induced upstream of the deflector, and especially (with an off-axis kick) between the deflector and the screen. Finally, the exact correlation induced by the deflecting structure depends on the precise momentum profile along the bunch. If the momentum variation along the bunch is linearly correlated in time (as is typical before and frequently after a magnetic bunch compressor), the final *x*-*z* correlation will be dependent on the sign of the slope of the rf deflecting voltage (i.e. *dV*/*dz*). This dependence is implicit in Eq. (7) and is made explicit by substituting: $p = p_0(1 + \Delta p/p_0)$, where we ignore the beta function and phase advance dependence on momentum. If the relative momentum deviation is linearly correlated in time along the bunch (i.e. $\Delta p/p_0 = \alpha z$, where α is the correlation factor), and a centroid deflection is included (i.e. $\varphi \neq 0$), the measured beam size is dependent on the sign of the momentum-time correlation. This is made explicit from Eq. (7), with the approximate momentum substitution, $1/p \approx (1 - \alpha z)/p_0$, and again forming the rms from the expectation values.

$$\sigma_x(\sigma_\delta) \approx \frac{2\pi}{\lambda}\frac{|eV_0|}{pc}\sigma_z\sqrt{\beta_d\beta_s}\,\left|\sin\Delta\psi\cos\varphi\right|\left[\left(1-\frac{\sigma_\delta}{\sigma_z}\frac{\lambda}{2\pi}\tan\varphi\right)^2+\frac{4}{5}\sigma_\delta^2\right]^{1/2} \qquad (14)$$

Here the (linearly correlated) rms relative momentum spread in the deflector is indicated by σ_δ, and (insignificantly) a uniform temporal distribution is assumed, which always has moments given by: $\langle z\rangle = \langle z^3\rangle = 0$ and $\langle z^4\rangle = 9\sigma_z^4/5$. The correlation factor is replaced by $\alpha \approx \sigma_\delta/\sigma_z$, assuming linearity, and that the uncorrelated component of momentum spread is insignificant. Finally, we have ignored σ_{x_0}, assuming, for simplicity, Eq. (10) is well satisfied.

Eq. (14), for typical parameters, can be reduced to a simpler form by ignoring the small $4\sigma_\delta^2/5$ correction term at far right. Ignoring this term also makes the next result independent of the type of temporal distribution.

$$\sigma_x(\sigma_\delta) \approx \frac{2\pi}{\lambda}\frac{|eV_0|}{pc}\sigma_z\sqrt{\beta_d\beta_s}\,\left|\sin\Delta\psi\cos\varphi\left(1-\frac{\sigma_\delta}{\sigma_z}\frac{\lambda}{2\pi}\tan\varphi\right)\right| \qquad (15)$$

Eq. (15) looks identical to Eq. (9), for small σ_{x_0}, except for the $\tan\varphi$ momentum spread correction term. It shows that, for a linearly correlated momentum spread, the measured beam size is dependent on the sign of the rf slope (*i.e.* $\tan\varphi$; see simulations for numerical examples). This appears to be a problem for the accurate determination of the bunch length, but can be mitigated in either of two ways. The first is to set $\varphi = 0$ or π, which

requires an on-axis screen, but eliminates the momentum spread dependent term. The second is to measure the spot size for two phases: $\varphi = \varphi_0$ and $\varphi = \pi - \varphi_0$, and average the two. The average spot size, along with the nominal spot size, is then used in Eq. (13) to calculate the bunch length, σ_z. The validity of this averaging is seen in Eq. (15) by replacing the function of the absolute value brackets with two separate equations for σ_x; one for $\varphi = \varphi_0$ and one for $\varphi = \pi - \varphi_0$. The mean value of σ_x is then equal to Eq. (9).

This same problem, and same solution, apply to the biasing effects of transverse wakefields. The wakefields install a fairly linear *x*-*z* correlation along the bunch, very similar to the momentum spread effect, which can also be cancelled by using the two-phase measurement and averaging. These wakefield and momentum spread effects are included in the detailed tracking simulations described below.

5 Application in the LCLS

The best location for an 8-foot long deflecting structure in the LCLS is downstream of the second bunch compressor where the bunch length is shortest, but not far downstream so that the beam momentum is still relatively low. Since we would also like to diagnose the effects of coherent synchrotron radiation (CSR) in the second compressor, it is best to install the structure as a vertical deflector so that CSR-induced correlations between horizontal position and time might be measured (the compressor is composed of horizontal bends). A similar idea for measuring the CSR-induced time-correlations using vertical momentum dispersion has also been suggested [10]. We should place the deflector near a defocusing quadrupole magnet where the vertical beta function is large. Since there is some available space at the end of 'linac-sector-25' where a screen can be installed, we locate the deflector approximately 60˚ in vertical betatron phase advance upstream of this screen location. The choice of 60˚ rather than 90˚ is used to reduce the effects of transverse wakefields on the bunch as it moves off-axis from deflector to screen. This argument is best understood by examining Figure 3, which shows the vertical trajectory after a 20-MV rf deflector at $\varphi \approx 3.3^\circ$.

The deflector and screen locations are indicated. This arrangement leaves a phase advance of $\Delta\psi \approx 60^\circ$. This can be increased to 90˚ by moving the screen downstream to the point where the trajectory is a maximum. The gain in deflector efficiency, however, is only ~10 % and the bunch stays well off-axis for an additional 25 meters, which amplifies the transverse wakefields induced in the accelerating structures. For this reason, the 60˚ location of '25-5A' is chosen for the deflector and '25-902' for the screen (these are the locations indicated in the figure). The existing 3-meter long accelerating structure at '25-5A' will be removed and the '25-5' klystron used to power the deflector.

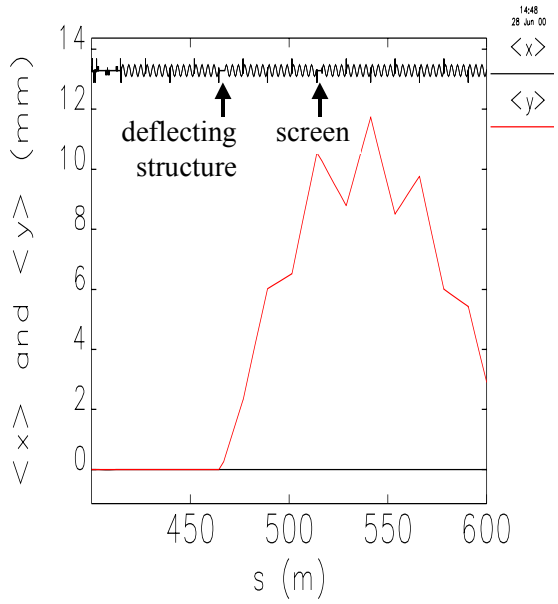

Figure 3. Vertical trajectory of beam centroid in LCLS for a 20-MV rf deflector at $\varphi \approx 3.3^\circ$. The second bunch compressor is located at far left in the plot. The trajectory amplitude used here is an extreme case.

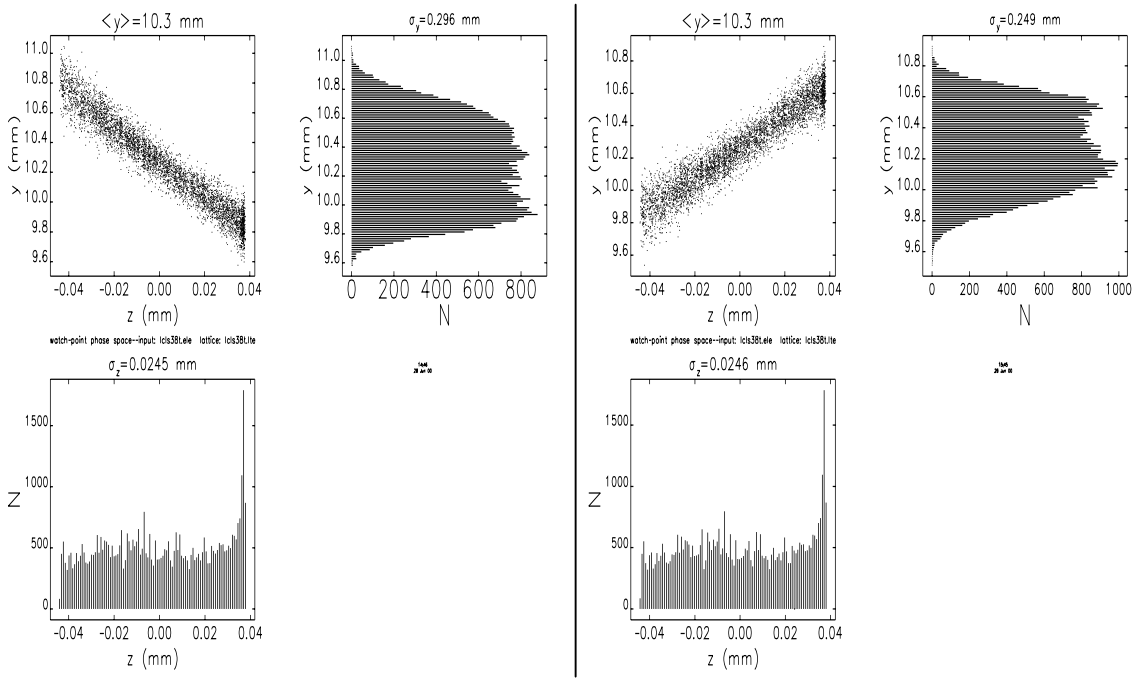

Figure 4. Vertical vs. longitudinal space in LCLS for $\varphi = 3.3^\circ$ (left) and for $\varphi = \pi - 3.3^\circ$ (right). The rms beam size on the screen varies from 296 μm (left) to 249 μm (right), due to wakes of the 1-nC charge, and a time-correlated rms momentum spread of 0.6 %. The two-phase averaging technique mitigates these effects (bunch head at left where $z < 0$).

Figure 4 shows the effect of the 20-MV vertical deflector for the case with $\varphi \approx 3.3^\circ$ and for $\varphi \approx \pi - 3.3^\circ$. The parameters are those given in Table 1. The figure is split in two parts and shows three plots per side. At upper left is the bunch population in *y*-*z* space. At upper right and lower left are the vertical and temporal (*z*) projected distributions, respectively (note the 24 μm rms bunch length). The particle tracking is performed using the computer code *Elegant*, written by Michael Borland at ANL [11], and includes wakefields, second-order optical effects of momentum deviations, and the sinusoidal time variation of the accelerating and deflecting rf fields.

Table 1. LCLS simulation parameters with an 8-foot long S-band deflecting structure.

Parameter	**symbol**	**value**	**unit**
RF deflector voltage	V_0	20	MV
Peak input power	P_0	25	MW
RF deflector phase (crest at 90°)	φ	3.3	deg
Nominal beam size	σ_{x_0}	80	μm
Beam size with deflector on (two-phase mean)	σ_x	272	μm
Beta function at deflector	β_d	58	m
Beta function at screen	β_s	63	m
Betatron phase from deflector to screen	$\Delta\psi$	60	deg
Normalized rms emittance	ε_N	1	μm
Beam energy at deflector	E_d	5.4	GeV
Beam energy at screen	E_s	6.2	GeV
RMS bunch length	σ_z	24	μm

The sign of the induced *y*-*z* correlation is flipped, and the measured beam size is changed by switching phases (as in Eq. (15), but also including wakefields), but the centroid kick is not changed [see Eq. (8)]. The time-correlated rms momentum spread used here is 0.6 % (bunch head lower energy than tail). By averaging the two beam size measurements, the bunch length can be accurately calculated without any significant bias form the wakefield or momentum spread effects shown here. The accuracy of this averaging technique can also be cross-checked by moving the screen on-axis and setting the rf phase to zero. A remotely moveable screen is therefore a desirable feature.

The rms bunch length of 24 μm is accurately calculated from this simulation using the average of the beam sizes in Figure 4, the parameters of Table 1, and Eq. (13), where $E_d \approx 5.4$ GeV and $E_s \approx 6.2$ GeV. With the *nominal* spot size also measured on the same screen (by switching off the rf deflector and moving the screen on-axis, or by setting the phase on rf crest at reduced voltage), the *nominal* distribution can be deconvolved from the vertical distributions in Figure 4, and the temporal distribution can be reconstructed

with significant precision at scales approaching 20 fsec. Even without the deconvolution, some of the temporal distribution is already evident in the measured vertical distribution.

Figure 5 shows a simulation of the screen's *x*-*y* images with deflector off and on. The effect of the deflector is very clear. In this case, there are no misalignments upstream of the deflector, so the horizontal and vertical emittances are the nominal value of 1 μm.

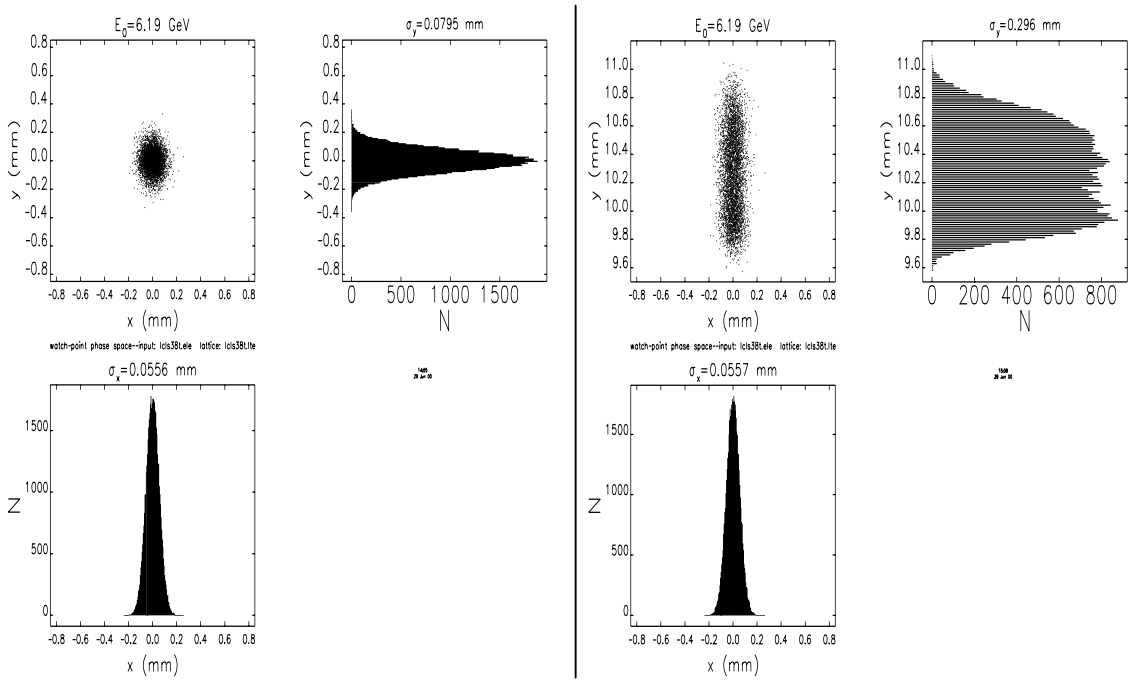

Figure 5. Vertical vs. horizontal space on LCLS screen for $V_0 = 0$ (left) and for $V_0 = 20$ MV (right). The rms vertical beam size on the screen is 80 μm (left) and 296 μm (right). The are no misalignments here.

Figure 6 shows the same simulated *x*-*y* screen images, but in this case there are large misalignments of the accelerating structures in the 350-meter long linac, upstream of the second bunch compressor (which is upstream of the deflector). The misalignments are large enough (500 μm rms) to generate nearly a factor of two emittance growth (a very pessimistic set of misalignments for the LCLS). The effects of the wakefields on the horizontal beam size can be seen in both scatter plots, but the horizontal time-correlation becomes evident on the plot at right with deflector on. The deflector is useful here as a way to measure the 'slice' emittance in the plane perpendicular to the deflection. A similar image might represent the effects of CSR. Using the two-phase averaging method, the upstream wakefield effects do not bias the bunch length measurement results.

The phase stability tolerance for the deflector is quite tight. If the phase varies by 0.1˚ (not uncommon), the mean vertical beam position on the LCLS screen varies by 0.3 mm.

For a single-shot measurement, however, good stability of the mean position is not critically required, and in addition, the calculated bunch length in Eq. (13) is very insensitive to the precise phase near the zero-crossing. In fact, with sufficient phase stability or with independent phase measurement, the variation of the mean position on the screen (from shot to shot, or by varying some interesting upstream parameter) can be used to diagnose the variation in beam arrival time at the deflector. Such a timing measurement can, for example, be used to measure the value of the R_{56} in the upstream chicane(s).

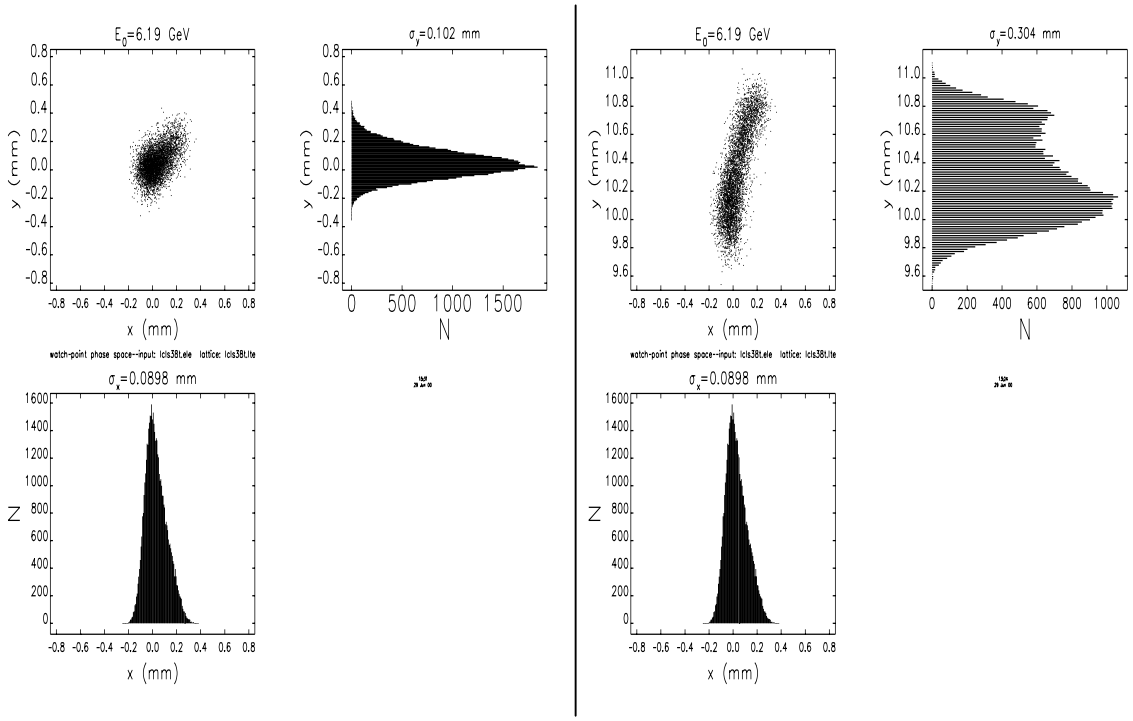

Figure 6. Vertical vs. horizontal space on LCLS screen for $V_0 = 0$ (left) and for $V_0 = 20$ MV (right). The rms vertical beam size on the screen is 102 μm (left) and 304 μm (right). In this case, there are large misalignments included upstream of the deflector which generate nearly a factor of two emittance increase.

6 Application in the SLAC Linac with Damping Ring

The same deflecting structure can also be applied to the existing SLAC linac. With a bunch length of 600 μm (in its shortest configuration) and a vertical emittance from the uncoupled damping ring of 5 μm, an S-band deflector can be very efficient. Table 2 lists some possible parameters for an 8-foot vertical deflector in the SLAC linac.

The deflector is located in linac-sector-29 at '29-4D' and the screen is located at '29-902'. This is ideal, since no accelerator section is presently located at '29-4D' and a remotely moveable screen, and associated controls, already exist at '29-902'.

Table 2. SLAC linac parameters with uncoupled damping ring injector at 1 nC of bunch charge.

Parameter	**symbol**	**value**	**unit**
RF deflector voltage	V_0	10	MV
Peak input power	P_0	6.5	MW
RF deflector phase (crest at 90°)	φ	17.9	deg
Nominal beam size	σ_{x_0}	68	μm
Beam size with deflector on (two-phase mean)	σ_x	575	μm
Beta function at deflector and at screen	$\beta_d = \beta_s$	53	m
Betatron phase from deflector to screen	$\Delta\psi$	77	deg
Normalized rms emittance	ε_N	5	μm
Beam energy at deflector and at screen	$E_d = E_s$	30	GeV
RMS bunch length	σ_z	600	μm

Figure 7 shows the simulation for this layout with a 10 MV, $\varphi \approx 18^\circ$ defector setting and a 30 GeV beam. The deflector-induced beam size on the screen is nearly ten-times larger than nominal, for an rf power input of just 6.5 MW into an 8-foot structure. With this overhead, beams with higher energies and larger emittance values can also be made to work adequately.

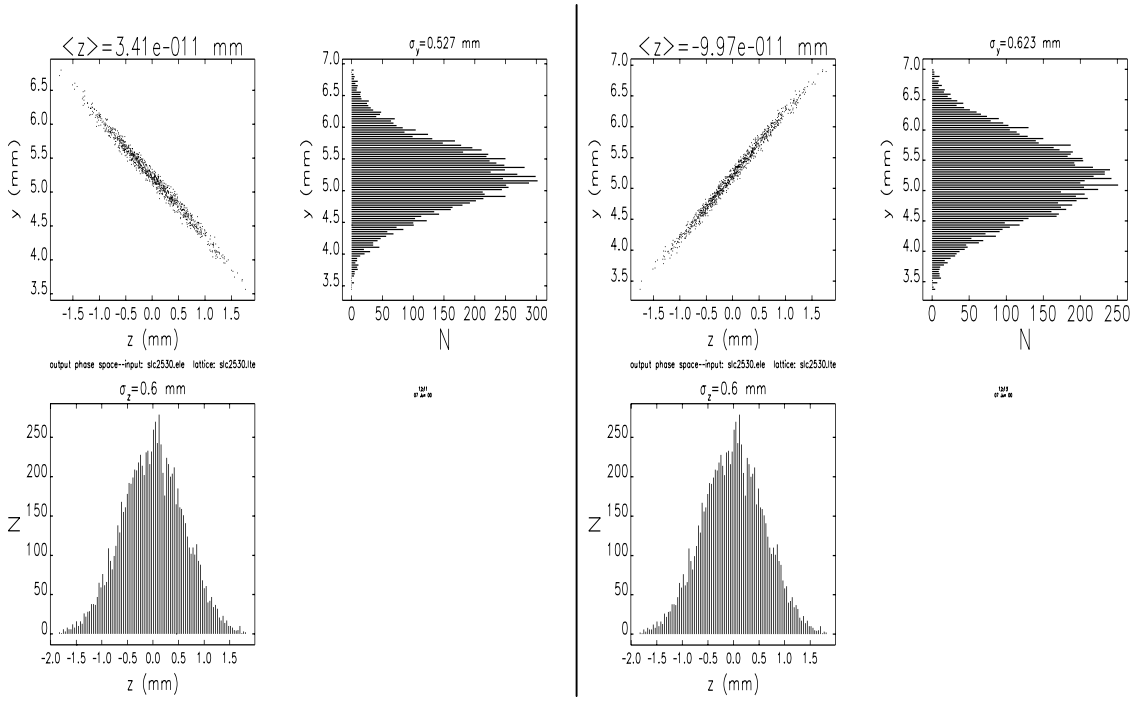

Figure 7. Vertical vs. longitudinal space for SLAC linac at $\varphi = 17.9^\circ$ (left) and $\varphi = \pi - 17.9^\circ$ (right). The rms beam size on the screen is 527 μm (left) and 623 μm (right), due to wakes of the 1-nC charge.

With the long bunch, care should be taken that the transverse wakefields generated between deflector and screen do not greatly bias the bunch length measurement results. The wakes are included in the simulation shown here, and are not a significant problem at 1 nC (6.2×10^9 ppb). At a much higher bunch charge the centroid offset might best be removed ($\varphi \approx 0$) and the screen moved on axis in order to alleviate the wakefield effect. The rms momentum spread used in this simulation is 0.6 % with a fairly linear correlation along the beam core (bunch head is at higher energy than tail).

It may also be interesting to use the existing vertical collimator at the '29-903' location (downstream of the deflector) to 'cut' the vertical spot size and therefore 'cut-down' the bunch length. Of course, the vertical pitch (*i.e.* the *y*-*z* correlation) will still be intact after the cut, so a second deflector would be needed downstream to remove this.

7 Application in the NLC

The same deflecting structure can also be applied to the NLC. With a bunch length of 90 μm (in the shortest NLC configuration) and an extremely small vertical emittance, an S-band deflector can be very efficient. Table 3 lists some possible parameters for the NLC solution.

Table 3. NLC parameters for an 8-foot long S-band deflector after the second bunch compressor chicane.

Parameter	**symbol**	**value**	**unit**
RF deflector voltage	V_0	20	MV
Peak input power	P_0	25	MW
RF deflector phase (crest at 90°)	φ	7.7	deg
Nominal beam size	σ_{x_0}	5	μm
Beam size with deflector on (two-phase mean)	σ_x	200	μm
Beta function at deflector and at screen	$\beta_d = \beta_s$	15	m
Betatron phase from deflector to screen	$\Delta\psi$	90	deg
Normalized rms emittance	ε_N	0.03	μm
Beam energy at deflector and at screen	$E_d = E_s$	7.9	GeV
RMS bunch length	σ_z	90	μm

The 8-foot long deflecting structure is located just after the bunch compressor chicane at 7.9 GeV, where the beta functions peak at 15 meters. The screen could be located just 90° downstream from here, also at a beta function of 15 m. Since there are no accelerating structures in this area, there are no transverse wakefield limitations between the deflector and the screen. The correlated energy spread effect in Eq. (15) is, however, significant ($\sigma_\delta \approx 1.6$ %) and the two-phase averaging is needed. The nominal vertical

beam size is 5 μm, while the average beam size measured with a 20 MV deflecting voltage is 200 μm. In this case, the nominal beam size is insignificant and no deconvolution is needed to resolve the temporal distribution.

8 Phase Space Diagnostic

As shown in Figure 6, the temporal structure of the horizontal emittance can be viewed using the vertical deflector. If at least two additional screens are added with appropriate horizontal phase advance, the horizontal slice emittance might also be measured. The vertical slice emittance could be measured by adding a second structure, as a horizontal deflector, where the horizontal beta functions are large.

The rf deflector can also be used to make a direct measurement of the details of the electron bunch population in longitudinal phase space. This is done by installing another screen, downstream of the deflector, at a location of large horizontal momentum dispersion. If the horizontal beta function is small enough, then the horizontal beam extent across the screen represents the momentum spread in the beam. By switching on the transverse rf as a vertical deflector and allowing the 'pitched' bunch to propagate to this new screen, the vertical extent across the screen represents the time axis along the bunch. This may require a zero-crossing rf phase (*i.e.* $\varphi = 0$ or $\varphi = \pi$) so that little or no trajectory kick is induced over the potentially long distance to the new screen. This also requires the vertical phase advance between deflector and dispersion screen to be approximately $\pi/2 + n\pi$. Figure 8 shows a simulation of this process through the LCLS, where the deflector is at the '25-5A' location, as described previously, and the screen is located 760-meters downstream at a location with momentum dispersion $\eta \approx 10$ cm and beta functions of $\beta_x \approx 1.8$ m, and $\beta_y \approx 10.7$ m. The beta functions are still large enough to wash out some of the temporal and momentum resolution, but the image is still a fairly good representation of the bunch population in longitudinal phase space.

9 Summary

The use of transverse deflecting structures to measure micro-bunch lengths in future FEL and linear collider projects looks quite promising. The measurements are absolute, require one or two beam pulses, and are based on measuring the electron beam size with an intercepting screen. Off-axis pulse-stealing schemes can be imagined which continually monitor the fine time structure of the bunch. More detailed phase space diagnostics can be arranged by adding additional screens at various betatron phases and/or locations of significant momentum dispersion. The immediate availability of several traveling wave S-band deflecting structures at SLAC makes their use of immediate interest for the LCLS, the NLC, and the present SLAC linac.

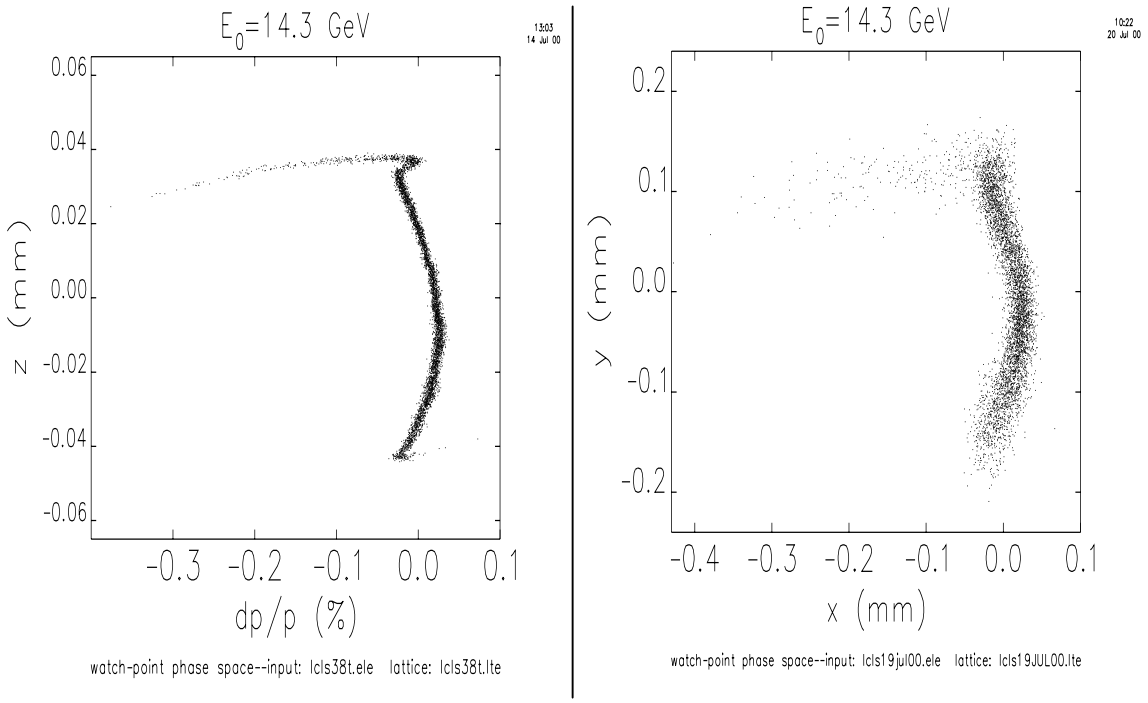

Figure 8. Longitudinal phase space population (left) [$\sigma_z \approx 24\ \mu$m, $\sigma_\delta \approx 0.04$ %] and its screen reconstruction (right) just prior to the LCLS undulator at 14.35 GeV, with rf deflector at 20 MV, $\varphi = 0$. The beta functions are still large enough to wash out some of the temporal and momentum resolution, but the image is still a good representation of the bunch population in longitudinal phase space (bunch head a bottom).

10 Acknowledgements

The authors would like to thank Theo Kotseroglou for pointing out the relevant work performed at SLAC in the 1960's. We would also like to thank Greg Loew and Xijie Wang for reminding us of the great potential in deflecting structures, and Ron Akre, Michael Borland and Mark Woodley for crucial technical support. Finally, we thank Max Cornacchia, Roger Miller, Marc Ross, and John Sheppard for encouragement and advice.

11 References

[1] G. A. Loew, O. H. Altenmueller, *Design and Applications of R.F. Deflecting Structures at SLAC*, PUB-135, Aug. 1965.

[2] R.H. Miller, R.F. Koontz and D.D. Tsang, *The SLAC Injector*, IEEE Trans. Nucl. Sci., June 1965, p804-8.

[3] I. Ben-Zvi, J. X. Qui, X. J. Wang, *Picosecond-Resolution 'Slice' Emittance Measurement of Electron-Bunches*, Proceedings of the 1997 Particle Accelerator Conference, Vancouver, BC, Canada, May 1997.

[4] O. H. Altenmueller, R. R. Larsen, and G. A. Loew, *Investigations of Traveling-Wave Separators for the Stanford Two-Mile Linear Accelerator*, The Review of Scientific Instruments, Vol. 35, Number 4, April 1964.

[5] *LCLS Design Study Report,* SLAC-R-521, (1998).

[6] *Zeroth-order Design Report for the Next Linear Collider*, SLAC-REP-474, May 1996.

[7] X.-J. Wang, *Producing and Measuring Small Electron Bunches*, Proceedings of the 1999 Particle Accelerator Conference, New York, NY, March 1999.

[8] G. A. Loew, private communication.

[9] H. Hahn and H. J. Halama, *Design of the Deflector for the R.F. Beam Separator at the Brookhaven AGS*, BNL-9306, 1965.

[10] D. Dowell, private communication.

[11] M. Borland, private communication.